

General properties of surface modes in binary metal-dielectric metamaterials

Sung Hyun Nam,¹ Erick Ulin-Avila,¹ Guy Bartal,¹ and Xiang Zhang^{1,2,*}

¹NSF Nanoscale Science and Engineering Center (NSEC),
3112 Etcheverry Hall University of California, Berkeley, California 94720-1740, USA

²Materials Sciences Division, Lawrence Berkeley National Laboratory,
1 Cyclotron Road Berkeley, California 94720, USA

*xiang@berkeley.edu

Abstract: We present general properties of surface modes in binary metal-dielectric metamaterials. We show mechanism for surface mode formation and analyze their existence conditions for semi-infinite metamaterials in the frame of couple mode theory.

©2010 Optical Society of America

OCIS codes: (240.6680) Surface plasmons; (160.3918) Metamaterials.

References and links

1. W. Shockley, "On the surface states associated with a periodic potential," *Phys. Rev.* **56**(4), 317–323 (1939).
2. S. G. Davison, and M. Steslicka, *Basic Theory of Surface States*, (Oxford Univ. Press, 1996).
3. N. Malkova, and C. Z. Ning, "Shockley and Tamm surface states in photonic crystals," *Phys. Rev. B* **73**(11), 113113 (2006).
4. K. Ishizaki, and S. Noda, "Manipulation of photons at the surface of three-dimensional photonic crystals," *Nature* **460**(7253), 367–370 (2009).
5. R. D. Meade, K. D. Brommer, A. M. Rappe, and J. D. Joannopoulos, "Electromagnetic Bloch waves at the surface of a photonic crystal," *Phys. Rev. B Condens. Matter* **44**(19), 10961–10964 (1991).
6. S. Foteinopoulou, M. Kafesaki, E. N. Economou, and C. M. Soukoulis, "Backward surface waves at photonic crystals," *Phys. Rev. B* **75**(24), 245116 (2007).
7. P. Yeh, A. Yariv, and A. Y. Cho, "Optical surface waves in periodic layered media," *Appl. Phys. Lett.* **32**(2), 104 (1978).
8. N. Malkova, I. Hromada, X. Wang, G. Bryant, and Z. Chen, "Transition between Tamm-like and Shockley-like surface states in optically induced photonic superlattices," *Phys. Rev. A* **80**(4), 043806 (2009).
9. S. H. Nam, E. Ulin-Avila, G. Bartal, and X. Zhang, "Deep subwavelength surface modes in metal-dielectric metamaterials," *Opt. Lett.* **35**(11), 1847–1849 (2010).
10. Y. Liu, G. Bartal, D. A. Genov, and X. Zhang, "Subwavelength discrete solitons in nonlinear metamaterials," *Phys. Rev. Lett.* **99**(15), 153901 (2007).
11. G. Bartal, G. Lerosey, and X. Zhang, "Subwavelength dynamic focusing in plasmonic nanostructures using time reversal," *Phys. Rev. B* **79**(20), 201103 (2009).
12. S. Feng, J. M. Elson, and P. L. Overfelt, "Optical properties of multilayer metal-dielectric nanofilms with all-evanescent modes," *Opt. Express* **13**(11), 4113–4124 (2005).
13. J. Yang, X. Hu, X. Li, Z. Liu, X. Jiang, and J. Zi, "Cancellation of reflection and transmission at metamaterial surfaces," *Opt. Lett.* **35**(1), 16–18 (2010).
14. S. H. Nam, A. J. Taylor, and A. Efimov, "Diaboliocal point and conical-like diffraction in periodic plasmonic nanostructures," *Opt. Express* **18**(10), 10120–10126 (2010).
15. P. Yeh, *Optical waves in layered media*, (John Wiley & Sons, 1988).
16. E. N. Economou, "Surface plasmons in thin films," *Phys. Rev.* **182**(2), 539–554 (1969).
17. X. Fan, G. P. Wang, J. C. W. Lee, and C. T. Chan, "All-angle broadband negative refraction of metal waveguide arrays in the visible range: theoretical analysis and numerical demonstration," *Phys. Rev. Lett.* **97**(7), 073901 (2006).
18. R. F. Oulton, V. J. Sorger, D. A. Genov, D. F. P. Pile, and X. Zhang, "A hybrid plasmonic waveguide for subwavelength confinement and long-range propagation," *Nat. Photonics* **2**(8), 496–500 (2008).
19. J. Klos, "Conditions of Tamm and Shockley state existence in chains of resonant cavities in a photonic crystal," *Phys. Rev. B* **76**(16), 165125 (2007).

1. Introduction

Understanding of localized states on the materials' surfaces is crucial to understand a multitude of physical and chemical phenomena occurring on the surfaces. Owing to the pioneering works by Tamm and Shockley and following numerous efforts, the origin and nature of the surface states has been revealed [1,2]. Optical analogues of the surface states

also have been studied in photonic lattice systems such as photonic crystals [3–6] and optical waveguide arrays [7,8]. The photonic lattices provide ideal and controlled environments for investigating surface modes, which have enabled new approaches to photon manipulation. Localized modes also can be supported on the surface of metamaterials made of metal-dielectric multilayers, leading to deep subwavelength mode profiles [9]. Such surface modes supported either in solids or in photonic lattices are formed by termination of the periodicity and can be categorized into two types, Tamm and Shockley states: while Tamm states appear due to strong perturbation above a certain threshold at the surface, Shockley states requires a different condition, break of the stronger bonding (coupling) at the surface in the chains of two alternating weak and strong bondings. In a band diagram, Shockley states show up in an inverted bandgap which is formed with crossing of adjacent bands.

The metal-dielectric metamaterials offer intriguing platforms for investigating surface modes. Weak and strong (binary) couplings for formation of Shockley-like modes can be realized not only with different strengths but also with combinations of signs for the two coupling coefficients, which have not been realized in the previous configurations [9]. In this paper, we present the origins of the surface mode formation arising from termination of the periodicity and identify their existence conditions in metal-dielectric metamaterials. We describe how internal interactions and surface perturbations affect the formation of surface modes in semi-infinite metamaterials through a simple model, which also allows clear physical insight into the localized modes in general photonic systems.

2. Internal interactions & band crossing in binary metamaterials

We begin by describing unique bulk properties of infinite binary metamaterials in Fig. 1(b) and 1(c) via comparison with conventional metal-dielectric metamaterials in Fig. 1(a). The metal-dielectric multilayers in Fig. 1(a) have been studied as metamaterials for subwavelength imaging and focusing since we can tailor their dispersions at will by adjusting layer parameters [10–14]. For the conventional structure in Fig. 1(a), the effective medium dispersion curve $k_x^2 / \varepsilon_{\parallel} + k_z^2 / \varepsilon_{\perp} = k_0^2$, where $\varepsilon_{\perp}^{-1} = \sum_i f_i \varepsilon_i^{-1}$ and $\varepsilon_{\parallel} = \sum_i f_i \varepsilon_i$ for electric fields acting along the direction normal and parallel to the layer plane and f_i is a filling ratio of the i th layer, agrees well with the accurate dispersion calculated by the transfer matrix method [15] for small κ ($= k_x \Lambda$, Λ is the lattice period). However, this approach can break down for the structures that have multiple interactions between constituents in metamaterials. Since the effective medium parameters are obtained by macroscopically averaging out electromagnetic properties of each constituent, internal microscopic features are not fully taken into account. Figure 2(d)–2(h) display the microscopic details for the coupling between surface plasmon polariton (SPP) modes in the layers [16]. The single gap SPP mode (TM polarization) in Fig. 2(d) couples to the adjacent identical mode through a thin metal layer as shown in Fig. 2(e), which causes mode splitting into symmetric and antisymmetric mode. For this case the propagation constant of the antisymmetric mode (β_a) is bigger than that of the symmetric mode (β_s) unlike conventional index-guided waveguides. Thus the corresponding coupling coefficient defined by $C = (\beta_s - \beta_a) / 2$ is negative (anomalous coupling) [17]. Now let us consider the structure in Fig. 1(b). The multilayer is similar to the one in Fig. 1(a) except for the alternating metal layer thicknesses, 40nm and 20nm, which leads to two different strengths of the couplings between adjacent SPP modes. As a result, two split dispersion curves are obtained. We can easily notice that the dispersion by effective medium approximation fails, even for small κ . Similar effect is observed with the structure in Fig. 1(c), whose unit cell consists of one metal layer (20nm) and three dielectric layers, consecutively $n = 1.34$ (50nm), $n = 3.48$ (200nm), and $n = 1.34$ (50nm) supporting single hybrid SPP mode as seen Fig. 2(f) [18]. Although the structure looks more complicated than the one in Fig. 1(b), there are also two types of couplings between SPP modes through the high index dielectric layer [normal coupling, $C > 0$, Fig. 1(g)] and through the metal layer

[anomalous coupling, $C < 0$, Fig. 1(h)]. Thus, the resulting two dispersion curves with huge splitting cannot be approximated by the single effective medium curve in Fig. 1(c). The examples in Fig. 1(b) and 1(c) clearly demonstrate the effect of the multiple interactions in metamaterials, which also plays an essential role in supporting surface modes in metal-dielectric metamaterials.

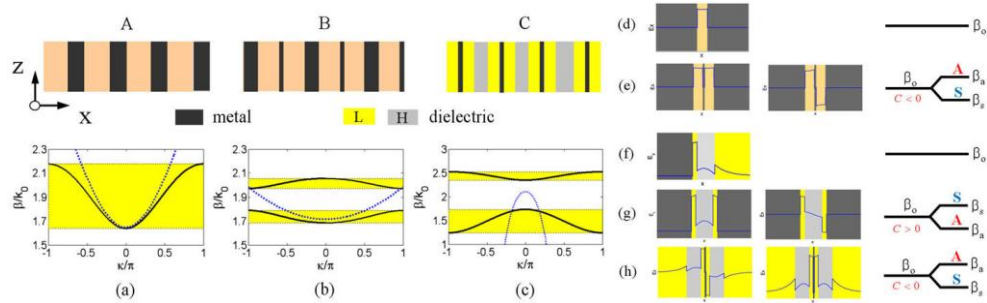


Fig. 1. (a)-(c) Three types of metal-dielectric metamaterials and the corresponding dispersion curves for the unit cell parameters (a) metal (Au, 20nm, dark grey) and dielectric ($n = 1.5$, 100nm, light orange), (b) metal 1 (Au, 20nm), metal 2 (Au, 40nm), and dielectric ($n = 1.5$, 100nm), (c) metal (Au, 20nm), dielectric 1 ($n = 1.34$, 50nm, yellow), dielectric 2 ($n = 3.48$, 200nm, light grey), and dielectric 3 ($n = 1.34$, 50nm). L: low index, H: high index dielectric. κ is the transverse wave vector multiplied by the lattice period Λ . The excitation wavelength is 1550nm. (d)-(e) Normal and anomalous coupling between two coupled SPP modes in metal-dielectric multilayers. Blue curves indicate transverse electric fields (E_z). (d) single SPP mode in a metal-dielectric-metal layer, (e) symmetric and antisymmetric mode by anomalous coupling of two gap SPP modes through a thin metal layer, (f) single hybrid SPP mode in a metal-three dielectric layer (low index/high index/low index), (g-h) symmetric and antisymmetric hybrid SPP modes by normal coupling through a high index dielectric layer and by anomalous coupling through a thin metal layer, respectively. The diagrams in the right display schematic mode splitting in the propagation constant.

For the binary metamaterials in Fig. 1(b) and 1(c), the band structure evolves with the relative strength of the couplings between SPP modes. We define asymmetry constant as the ratio of coupling coefficients, $\eta = C_- / C_+$. The asymmetry constant η can take both negative and positive values depending on the sign of C_+ and C_- . For example, η is positive for the structure in Fig. 1(b) and negative for the one in Fig. 1(c) [9]. The evolutions of bands are shown in Fig. 2(a)–2(c) for the structure in Fig. 1(c) with increasing magnitude of η . To control the magnitude (through C_-), we adjust the thickness of the metal layer to 15nm, 8.4nm, and 5nm, respectively. The thickness of the other layers is fixed (see the figure caption). The thinner the metal layer, the stronger the coupling becomes, thus $|C_-|$ increases. The evolution of two-band structure as a function of η is simplified in Fig. 2(d) by coupled mode theory [2,9]. With $\eta = 0$, we obtain only two discrete values corresponding to the symmetric and antisymmetric modes from the normal coupling (C_+) with no band formation [two red circles in (d)]. As the magnitude of η increases, the bandwidth linearly increases until $|\eta| = 1$. The bandgap with $|\eta| < 1$ is a direct bandgap [the yellow region D in (d)]. Figure 2(a) corresponds to this case. The coupling through the metal layer ($d_{\text{Au}} = 15\text{nm}$) is not strong enough yet, so η is in the range of $-1 < \eta < 0$ and the bandgap is direct. The eigenmodes at the bandedges B and T are shown in Fig. 2(e) and 2(f), respectively. With reduced metal thickness (8.4nm from 15nm), C_- is increased and reaches the same magnitude as C_+ ($\eta = -1$). The bandgap is closed [Fig. 2(b)] at $\kappa = 0$ and the eigenmodes in (e) and (f) become degenerate. The touching point becomes a singularity [green arrow in (b)] called diabolical point or Dirac point. It brings important consequences for the light propagation dynamics in the nano-scale as the intersection of energy bands (conical intersection) has great importance

for molecular dynamics and electron transport [14]. As η increases more ($|\eta| > 1$), the two bands cross and an inverted bandgap appears [grey region in (d)]. As a consequence of the band crossing, the eigenmodes at the bandedges are interchanged. Figure 2(c) shows a crossed band with $\eta < -1$ when the metal layer thickness is more reduced to 5nm and $|C_-|$ further increases. The crossed band can be easily identified by the eigenmodes at the bandedges. We can observe the exchanged eigenmode symmetry at B' and T' in Fig. 2(g) and 2(h). The band crossing feature in the binary metamaterial is analogous to the electronic band crossing for the chain of atoms with s- and p- orbitals [2]. The band crossing phenomena is one of the essential features of binary metamaterials and causes a direct consequence on the formation of surface modes.

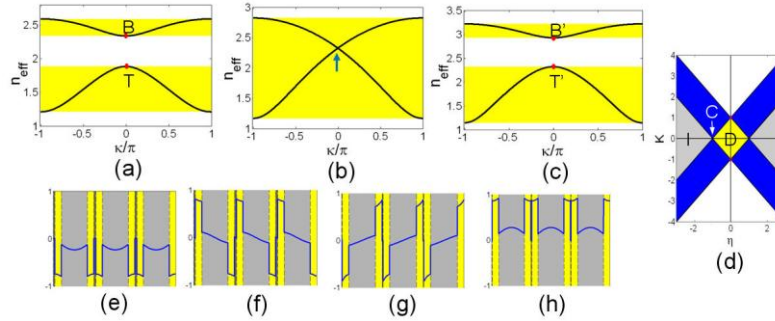


Fig. 2. Bandgap closing & band crossing. (a), (b), (c) Band diagrams for the metal (Au) layer thickness $d_{Au} = 15\text{nm}$ (a), for $d_{Au} = 8.4\text{nm}$ (b), and for $d_{Au} = 5\text{nm}$ (c). The thickness of the other layers is kept as $d_{MgF2} = 50\text{nm}$ and $d_{Si} = 200\text{nm}$. B, B': band edges of the upper bands, T, T': band edges of the lower bands in (a) and (c). The arrow in (b) indicates the singular point. (d)

Band evolution calculated by coupled mode theory as a function of η . The bands are marked in blue, the direct bandgap (D) in yellow, and the inverted bandgap (I) in grey. The arrow in (d) marks the bandgap closing point C at $\eta = -1$. (e-h) Eigenmodes at the bandedges B (e), T (f), B' (g), and T' (h), respectively.

3. Formation of surface modes and their existence condition

When the periodicity is terminated, localized modes whose amplitudes decay away from the surface can be supported. To analyze the existence conditions of the surface modes, we describe their formations based on coupled mode theory. For a semi-infinite metamaterial with termination of C_- coupling on one side as seen at the top in Fig. 3(c), the governing coupled differential equations for the bulk are given by Eq. (1):

$$\left(i \frac{\partial}{\partial z} + \beta_0 \right) a_n + C_- b_{n-1} + C_+ b_n = 0, \quad \left(i \frac{\partial}{\partial z} + \beta_0 \right) b_n + C_+ a_n + C_- a_{n+1} = 0, \quad (1)$$

where β_0 is the propagation constant of the SPP mode in an isolated unit cell, and a_n and b_n are the field amplitudes of the n th odd-numbered and even-numbered SPP modes from the surface of binary metamaterials, respectively. Next we apply the boundary condition on the surface $(i\partial/\partial z + \beta') a_1 + C_+ b_1 = 0$, where β' is the propagation constant of the surface mode, and a_1 and b_1 are the amplitudes for the first and second SPP modes from the surface, respectively. For trial solutions, we use $a_n = p_n e^{i\beta z}$ and $b_n = q_n e^{i\beta z}$ where $p_n = p_0 r^{n-1}$ and $q_n = q_0 r^{n-1}$. For the localized modes decaying away from the surface, the condition $|r| < 1$ must be met. By inserting the ansatz into Eq. (1), we obtain as below:

$$q_0 = (K + Z) p_0 - K p_0 + \left(\frac{\eta}{r} + 1\right) q_0 = 0, \quad -K q_0 + (\eta r + 1) p_0 = 0, \quad (2)$$

where we introduce new parameters, dimensionless propagation constant and surface perturbation, $K = (\beta - \beta_0) / C_+$ and $Z = (\beta_0 - \beta') / C_+$, respectively. Depending on the existence of surface perturbation, we have two scenarios for the surface modes. Here we will describe only negative η case and extension to positive η case is straightforward.

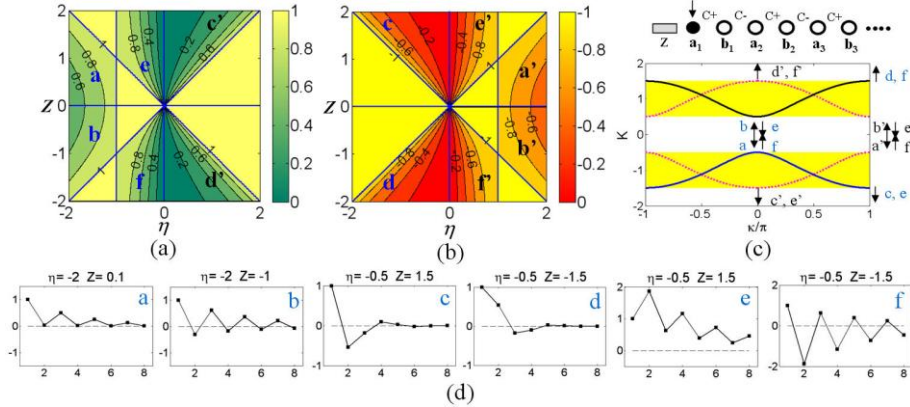


Fig. 3. (a) Existence conditions for surface modes in $\eta - z$ plane corresponding to the plus solution in Eq. (3). The contours with constant r indicate degree of localization. (b) Existence conditions corresponding to the minus solution in Eq. (3). (c) Top: A schematic for semi-infinite binary metamaterials with termination of C- coupling at the left end. The a_n and b_n indicate amplitudes of SPP modes at n th even-numbered and odd-numbered SPP modes from the surface, not the physical layers. The arrow and Z indicate the location of surface and the surface perturbation, respectively. Bottom: Band diagram for positive (red dotted) and negative (solid) η , and shift of the surface mode locations in the band diagram with increasing surface perturbation Z . (d) The corresponding eigenvectors for the surface modes in the regions **a-f** marked in (a) and (b).

- (1). *No surface perturbation* ($z = 0$): We obtain $K = 0$, $q_0 = 0$, and $r = -1/\eta$ from the Eq. (2). Thus we have localized surface modes at the center of the bandgap ($\beta = \beta_0$) under the condition of $|\eta| > 1$. This localized mode corresponds to the Shockley states in condensed matter. This mode appears only in the inverted bandgap, meaning that the stronger coupling (C_-) is terminated at the surface. Only the odd-numbered SPP modes (a_n) are non-zero.
- (2). *With surface perturbation* ($Z \neq 0$): For this case, the following solution is obtained for r from Eq. (2).

$$r = \frac{1}{2} \left(\left(\frac{\eta^3}{Z^2} - \eta \right) \pm \sqrt{\left(\frac{\eta^3}{Z^2} - \eta \right)^2 + 4 \left(\frac{\eta}{Z} \right)^2} \right). \quad (3)$$

For localized mode solutions, the allowed ranges of two parameters, η and Z are identified in Fig. 3(a) and 3(b) from the two solutions in Eq. (3). The contours for constant r indicate the degree of localization; the smaller values, the stronger localization. Depending on the combination of η and Z , the whole plane is divided into several regions. The existence and character of the surface modes is determined by which region the modes belong to. We describe the detailed properties of the modes in each region below.

- (i) $-1 \leq \eta \leq 0$ & $Z \leq |\eta|$: In this region no surface mode exists. The bandgap is direct and the surface perturbation is too weak to induce surface modes.
- (ii) $-1 \leq \eta \leq 0$ & $Z > |\eta|$ (the region **e** and **f**): Tamm-like surface modes are supported due to strong surface perturbations. Two different types of solutions are obtained in this region. One of these is located in the center bandgap. These Tamm-like modes move toward the center from the bandedges with increasing surface perturbations. The other type of solution is located out of the bands (not between) and move away from the band edges with increasing perturbation. Since those two types are located in different positions in the band diagram, their mode symmetries are also different. The mode profiles for those located in the center bandgap are shown in Fig. 3(d) for opposite signs of Z . The mode energy is more localized in the even-numbered SPP modes (b_n).
- (iii) $\eta \leq -1$ & $Z < |\eta|$ (the region **a** and **b**): Although surface perturbation is weak, Shockley-like modes are supported due to the break of stronger coupling. The increase of surface perturbation $|Z|$ makes the surface modes more delocalized until it reaches the line of $Z = \pm\eta$ where the modes become extended, which is in sharp contrast to the region $-1 < \eta < 0$ where the modes need strong surface perturbation ($|Z| > |\eta|$) to be localized. The shift of mode locations in Fig. 3(c) also confirms this. The modes move toward the bandedges from the bandgap center with increasing perturbation. The corresponding eigenmode profiles are also shown in Fig. 3(d). The mode energy is localized only in a_n SPP modes without surface perturbation and the field amplitude decays into the bulk without changing the sign. With increasing perturbation, the mode energy in b_n SPP modes starts to increase.
- (iv) $\eta \leq -1$ & $Z > |\eta|$ (the region **c** and **d**): Shockley-like modes do not exist in this strong perturbation region but Tamm-like modes can be supported. The modes are located out of the bands and move away from the bandedges with increasing perturbation. The corresponding eigenmodes shown in Fig. 3(d) change the sign of the field amplitude at every other SPP modes.

The mode symmetries for positive η are opposite compared to the case of negative η due to the flipped band curvatures. For finite metal-dielectric metamaterials with strong internal interactions, surfaces at each side can interact, thus can complicate the analysis [9,19]. Nevertheless the simple approach described in this paper sheds clear insight on the fundamental physics of the surface modes in metal-dielectric metamaterials.

5. Conclusion

We have analyzed how internal interactions and surface perturbations affect the formation of surface modes in binary metal-dielectric metamaterials. A simple model has been introduced to analyze the existence conditions and mode symmetries of the surface modes in semi-infinite metamaterials. The surface modes in metamaterials could be utilized for manipulating surface plasmon polaritons in the nano-scale.

Acknowledgements

This work has been supported by U.S. Army Research Office (ARO) MURI program 50432 PH-MUR.